Research Article

Adsorption Science & Technology
Volume 42: 1–18

DOI: 10.1177/02636174241287698
journals.sagepub.com/home/adt
Sage

Characterization and adsorption properties of rectorite/sludge-derived biochar composites for Pb(II) removal

Huanhuan Wang
School of Environment and Tourism, West Anhui University, Lu'an, China

Jing Wang
School of Resources and Environmental Engineering, Hefei University of Technology, Hefei, China

Zi Wang
College of Resources and Environmental Science, South-Central University for Nationalities, Wuhan, China

Qing Ye
School of Environment and Tourism, West Anhui University, Lu'an, China

Junye Zhang
School of Resources and Environmental Science, Wuhan University, Wuhan, China

Abstract

Clay-based adsorbent materials are widely used to remove heavy metal ions from water. In this study, we have fabricated a novel composite material, consisting of rectorite and sludge-derived biochar (REC/SDBC), and characterized its effectiveness in removing lead from water. Our SEM images show that the REC is evenly dispersed on the surface of the SDBC. The composites have a mesoporous structure, and its BET surface is (16.5 m^2/g) comparable with that of SDBC but larger than that of REC. We found that the maximum adsorption capacity for Pb(II) was 26.89 mg g^{-1} for REC/SDBC composites with a REC:SDBC ratio of 3:1, which was achieved within 120 min. This is higher than the adsorption capacities of REC (19.81 mg g^{-1}) and SDBC (23.15 mg g^{-1})

Submitted March 6, 2024; accepted September 12, 2024

Corresponding author:
Junye Zhang, School of Resources and Environmental Science, Wuhan University, Wuhan 430079, China.
Email: zhangjunye@whu.edu.cn

alone. Furthermore, we observed that the adsorption capacity was greater at pH 5.0 compared to other pH values. Our results also indicate that the pseudo-second-order model and the Langmuir isotherm model provide good fits for the rates and isotherms of Pb(II) adsorption onto REC/SDBC composites. The adsorption kinetic constant and the Langmuir adsorption constant were calculated to be 0.0065 g mg^{-1} min^{-1} and 0.319 L mg^{-1}, respectively. X-ray photoelectron spectroscopy analysis confirmed that the reaction mechanism is mainly dominated by chemisorption, involving cationic exchange, surface complexation, and surface precipitation. The high adsorption capacity, combined with the cost-effectiveness and environmental-friendly nature of REC/SDBC composites, make them promising candidates for removing heavy metallic elements from wastewater.

Keywords
rectorite, biochar, lead, adsorption, kinetics, mechanism

Introduction

A by-product of wastewater treatment plants is Sewage sludge (SS) and disposal of SS is a challenging issue because of its large quantities and considerable amount of hazardous contents including heavy metals, bacteria, fungi, and organic matter (Gao et al., 2020; Hoang et al., 2022; Xiao et al., 2018a). Traditional disposal methods, such as landfill, combustion, and anaerobic digestion, are expensive and may cause secondary pollution (Zhang et al., 2013). In order to promote resource utilization, the sludge needs to be treated in an environmentally sound manner (Fang et al., 2023). Pyrolysis is able to destroy or stabilize most microorganisms and toxic metals simultaneously (Liu et al., 2021), achieving the target of "reduce, reuse and safety" in SS disposal. Biochar, which refers to a carbonaceous solid byproduct of biomass pyrolyzed in the absence of oxygen, is an environmental-friendly substance with superior properties such as high surface-to-volume ratio and rich functional groups over the surface.

According to recent studies (Abdul et al., 2017; Edo et al., 2020; He et al., 2018; Xiao et al., 2018b; Zhou et al., 2017b), biochar is an ideal option for treating water in plants contaminated with organic or heavy metal pollutants. It has been shown to effectively remediate soil and has minimal impact on climate change through carbon sequestration, making it a more sustainable choice compared to traditional soil remediation methods (Cao et al., 2011; Woolf et al., 2010; Zhang et al., 2021). Additionally, biochar can be produced on a large scale using readily available materials and simple fabrication processes, from industrial facilities to individual farms (Damdib et al., 2023; Liu et al., 2015). As a result, the conversion of sludge to biochar through pyrolysis has become a popular research topic for sustainable sludge disposal. However, the relatively low functionality of biochar has limited its widespread application (Pan et al., 2021).

To address the issue of low efficiency in biochar, several engineering techniques have been utilized. These include surface activation through the use of chemical reagents such as alkali, acid, and oxidants (Song et al., 2018; Tang et al., 2018; Wang and Liu, 2018), as well as the loading of metal (metal oxides) and functional particles onto the surface of biochar to improve its adsorption capabilities (Abdul et al., 2017; Inyang et al., 2014; Kah et al., 2017; Liang et al., 2017). Rectorite (REC) is an interstratified clay that contains alternating layers of dioctahedral smectite and mica, but with a 1:1 expandable ratio (Zhang et al., 2010). Due to its ability to easily exchange organic and inorganic cations, such as Na^+, K^+, and Ca^{2+} (Wu et al., 2011), REC is highly effective in adsorbing heavy metals like lead (Pb). As a result, REC emerges as a

promising and reliable functional particle for the modification of sludge-derived biochar (SDBC). Specifically, SDBC has been selected as the supporting structure for the loading of REC particles onto its surface, with the aim of enhancing its physiochemical properties and improving its adsorption efficiency for the removal of Pb(II).

To date, only a few studies were conducted regarding the adsorption of contaminants by biochar-clay composites (Chen et al., 2017; Li et al., 2017c; Wang et al., 2017a; Yao et al., 2014). Biochar-clay composites are the preferred adsorbents for removing pollutants due to their cost-effectiveness and high adsorption efficiency.

Heavy metals enter the environment mainly in water, soil, and the atmosphere and migrate between them, contaminating a wide range of areas. The most serious contamination of soil and water, among many heavy metals (Abdulkarim and Abu Al-Rub, 2004; Tang et al., 2020), is lead (Pb), which is highly toxic, abundant, nonbiodegradable, and can accumulate in nature. Consequently, heavy metal pollution, including that of lead, threatens ecosystem health (Bordoloi et al., 2017; Liu et al., 2019; Wang et al., 2017b; Wu et al., 2018). Even dilute solution of Pb is particularly hazardous (Liu et al., 2019; Renu et al., 2021). Consequently, it is essential to develop efficient methods to treat solutions and resolve heavy metal pollution. Considering the high toxicity of lead, the necessity of developing effective removal methods is especially more pronounced for Pb. In this regard, numerous methods have been proposed so far. For example, adsorbents derived from industrial or agricultural waste products have a simple and low-cost production process (Dias et al., 2017; Lyu et al., 2018; Wang et al., 2018; Wu et al., 2017; Zhou et al., 2017b). It has been reported that clay minerals possessed high adsorption capacity for Pb (Uddin, 2017). Nevertheless, these studies were mostly focused on montmorillonite-derived adsorbents. Rectorite has a similar structure with montmorillonite but is cheaper than montmorillonite. There is no comprehensive investigation into the synthesis of REC/SDBC composites for removing Pb(II) in aqueous solutions.

In this study, we aim to utilize the byproduct SS from wastewater treatment plants as a low-cost source of clay minerals for the development of cost-effective REC/SDBC composites for removing heavy metals from water. Our specific objective is to evaluate the physiochemical properties of these composites, with a focus on their performance and mechanistic pathways for adsorbing Pb(II) in aqueous solutions. To achieve this, we conducted a thorough characterization of the synthesized REC/SDBC composites; studied their kinetics, equilibriums, and thermodynamic parameters; and analyzed their chemical states before and after adsorption. Our goal is to investigate the potential of REC/SDBC composites for adsorbing Pb(II).

Materials and methods

Materials

In this article, REC was prepared by Hubei Mingliu Inc., China. The SS was gathered at the Hunan, China's Yuelu Wastewater Treatment Facility. The SS was dried at 60 °C for 48 h before being put through a 60-grit sieve (0.3 mm). Moreover, $Pb(NO_3)_2$ with an analytical quality was prepared from Sonopharm Chemical Reagent Co., China. A stock solution of Pb(II) (500 mg g^{-1}, pH 2.0) was used in the experiment, the working solution with other Pb(II) concentrations was prepared by dilution. Every other chemical was of analytical quality and was used exactly as it was given (Electrical resistivity = 18.23 M Ωcm). Moreover, pure water was utilized to reduce aqueous solutions.

Preparation of REC/SDBC composites

Rectorite/SDBC composites were prepared using the method previously reported by Li et al. (2017c) and Chen et al. (2017). In summary, 2.4 g of REC powder was mixed with 60 mL of deionized (DI) water to create a stable REC suspension, which was then

sonicated for 30 min. The REC suspension was then combined with 0.8 g of pretreated SS biomass material and stirred for 2 h. The resulting mixture was separated, and the feedstocks were dried at 60 °C. Next, the feedstocks were heated in a tube furnace at a rate of 5 °C/min for 2 h under a N_2 environment. The resulting REC/SDBC composites had a REC to SS biomass mass ratio of 3:1 and were identified as such after being ground and passed through a 60-mesh sieve. Rectorite/SDBC composites with REC to SS biomass mass ratios of 5:1, 1:1, and 1:3 were also synthesized using the same procedure.

Characterizations

The morphology of the materials was assessed using FE-SEM (Zeiss SIGMA). Additionally, the elemental composition of REC/SDBC composites was determined using EDS (EDAX Genesis). Nitrogen adsorption at 77 K was measured using a BEL-SORP-Mini II analyzer. The surface area and adsorption–desorption isotherms of the specimens were calculated using the BET technique (Dias et al., 2018; Kah et al., 2017). The main elements (C, H, N, O) were quantified using a Vario EL cube elemental analyzer (Elemantar). The ash content was determined after 4 h of calcination at 600 °C, and the main metal contents of the samples were detected using XRF (Rigaku, ZSKprinus) (Li et al., 2018b). Heavy metal contents of the specimens were measured after acid digestion using ICP-MS (NexION 300X PerkinElmer). The crystallographic structure of the samples was characterized using XRD with Cu Kα radiation (D8 ADVANCE, Bruker AXS). The surface functional groups of the samples were identified using FT-IR (Nicolet 5700). The surface charge properties of the composites were measured using zeta potential measurements (Nano-ZS series Model ZEN3600, Malvern, UK). X-ray photoelectron spectroscopy (XPS) of the REC/SDBC composites before and after Pb(II) adsorption were obtained using a Thermo-Scientific Escalab 250Xi instrument with Al Kα irradiation of hv = 1486.6 eV as the X-ray source.

Batch adsorption experiments

Batch adsorption tests were conducted to investigate the performance and mechanism of Pb(II) adsorption using the prepared samples. The tests were carried out in 250 mL sealed conical flasks on a temperature-controlled rotary shaker at 150 rpm. A 100 mg of the samples (REC, SDBC, or REC/SDBC composites with different mass ratios of 5:1, 3:1, 1:1, and 1:3) were mixed with 100 mL of Pb(II) solution. The initial pH was adjusted to 5 ± 0.1 using 0.2 M HNO3 and NaOH solutions at a temperature of 20 ± 0.5 °C. To determine the kinetics parameters of adsorption in a 50 mg L^{-1} Pb(II) solution, 2 mL batches were sampled at different times (5–1440 min). The effect of pH on Pb(II) adsorption was studied at a pH range of 2–6, with the pH being adjusted using 0.2 M HNO_3 and NaOH solutions. Adsorption isotherm tests were also conducted at 293.15, 303.15, and 313.15 K for 24 h using Pb(II) concentrations of 10–500 mg L^{-1}. After the adsorption process was completed, 2 mL batches were sampled using a syringe and immediately filtered through a 0.22-μm membrane for Pb(II) concentration analysis.

A Purkinje General TAS-990 spectrometer (Beijing China) was used to measure the concentration of Pb(II) using the flame atomic absorption spectroscopy (AAS) method. To ensure accuracy, each test was repeated three times, and the average value was recorded to reduce relative errors to less than 5%. The adsorption capacity of Pb(II) is defined as equation (1), wherein C_0 and C_e are the initial and equilibrium concentrations of Pb(II), q_e refers to the adsorption capacity of adsorbent under equilibrium state, m is the weight of adsorbent and V denotes the total volume of solution:

$$q_e = \frac{(C_0 - C_e) \times V}{m} \tag{1}$$

Results

Characteristics of REC/SDBC composites

The physicochemical characteristics and elemental contents of SS, REC, SDBC, and REC/SDBC composites are presented in Tables 1 and 2, respectively. It can be observed that the yield value and ash content are high in SDBC and REC/SDBC composites, which can be attributed to the high inorganic mineral component present in these samples. This is due to the fact that REC is a type of clay mineral that remains stable at high temperatures, resulting in a higher yield value and ash content in REC/SDBC composites. The XRF results in Table 2 also indicate a significant amount of inorganic elements, such as silicon, aluminum, and Pb(II), in each sample. Additionally, it has been found that the amounts of C, H, N, and O in SDBC and the REC/SDBC composites are lower than those in the starting sludge (SS), yet the metal concentrations are comparatively higher. This phenomenon can be explained by the high-mineral biochar pyrolysis process, where the mineral enrichment outweighs the degree of carbonization (Li et al., 2018b; Park et al., 2018; Ren et al., 2018). The H/C ratio increases in SDBC and REC/SDBC composites, indicating a decrease in the degree of carbonization and the preservation of organic residues, such as polymeric CH_2 and fatty acids (Chen et al., 2008; Chen et al., 2012).

The morphological characteristics of REC, SDBC, and REC/SDBC composites are shown in Figure 1 using FE-SEM. It can be observed that REC has a lamellar structure (Figure 1(a)). The majority of SDBC particles are amorphous and granular, with a rough and porous surface (Figure 1(b)). In Figure 1(c), it can be seen that REC in REC/SDBC composites is dispersed on the surface of SDBC, with partial exfoliation also present in the lamellar structure. The EDS spectra of REC/SDBC composites are shown in Figure 1(d). The main components of the composites are C, O, Si, and Al, which are consistent with the elemental contents listed in Table 2. The interaction between REC and SDBC, as well as the uniform dispersion of REC, contributes to the improved adsorption capacity of heavy metals by REC/SDBC composites.

Figure 2 shows the adsorption–desorption isotherms for nitrogen molecules and the corresponding BJH pore size distribution of the REC, SDBC, and REC/SDBC composites. Table 1 displays the total pore volume, average pore width, and BET-specific surface area for each sample. According to the IUPAC classification, all N_2 adsorption–desorption isotherms exhibit type IV behavior with an H3 hysteresis loop (Huang et al., 2018; Xu et al., 2018; Zhang et al., 2013), indicating the presence of a mesoporous structure in the samples. This is also reflected in the pore size distribution. The specific surface area and average pore diameter of the REC/SDBC composites are lower than those of SDBC due to the deposition of REC on the surface of SDBC.

The XRD spectra of REC, SDBC, and REC/SDBC composites are shown in Figure 3. The peaks at $2\theta = 3.95°$ and 7.99° are characteristic of REC (Chen et al., 2015), while the peak at $2\theta = 20.04°$ is also attributed to REC (Yao et al., 2014). Sludge-derived biochar exhibits a characteristic peak at $2\theta = 26.6°$, indicating the presence of quartz as the main crystalline structure (Cao et al., 2011). A weak peak of Fe_2O_3 is also detected, suggesting a small amount of Fe_2O_3 in the SDBC samples (Li et al., 2018a). In the REC/SDBC composites, the peak at $2\theta = 7.99°$ disappears and the intensity of the peak at $2\theta = 3.95°$ decreases, indicating partial destruction of the ordered structure of REC (Wu et al., 2011). Additionally, the peak of quartz is observed but is weaker than in SDBC, indicating a decrease in quartz crystallinity in the composites.

In contrast to traditional biochar made from organic matter residues such as wheat straw (Yang et al., 2017), banana peel (Zhang et al., 2013), peanut shell (Bai et al., 2017), and pig manure (Dhyani et al., 2018), SDBC is a carbon-mineral composite that contains both mineral oxides and organic functional groups (Ren et al., 2018). While the surface functional

Table 1. Properties of REC and SDBC and REC/SDBC composites prepared in this work.

Samples	Yield (%)	Ash(%)	BET surface area ($m^2\ g^{-1}$)	Total pore volume (cm^3g^{-1})	Average pore diameter (nm)
SDBC	69.4%	80.16%	16.6	0.070	16.858
REC	/	/	6.0	0.033	22.163
REC/SDBC	86.91%	89.68%	16.5	0.056	13.669

Table 2. Elemental analysis of SS, REC, SDBC, and REC/SDBC composites.

	Organic elemental content (%)				Atomic ratio H/C
Samples	C	H	N	O	
SS	21.25	3.22	3.57	20.47	0.15
SDBC	13.07	2.67	1.76	12.03	0.20
REC	/	/	/	/	/
REC/SDBC	4.58	1.87	0.50	0.41	0.41

	Main metal content (%)						
	SiO_2	Al_2O_3	Fe_2O_3	CaO	MgO	K_2O	Na_2O
SS	/	/	/	/	/	/	/
SDBC	40.25	16.68	7.13	2.27	1.46	2.59	0.40
REC	45.62	37.87	2.92	3.60	0.52	1.44	1.40
REC/SDBC	42.47	31.85	3.63	2.91	0.69	1.57	1.10

	Heavy metal content ($mg\ kg^{-1}$)						
	Cu	Zn	Pb	Cd	Ni	Cr	Co
SS	278.00	764.50	50.85	1.95	26.50	502.00	30.30
SDBC	332.95	940.75	165.50	2.30	58.85	554.00	34.15
REC	31.25	62.65	19.60	2.60	26.65	1091.50	6.40
REC/SDBC	209.30	504.60	46.40	3.15	10.60	1122.50	9.90

groups of SDBC and REC/SDBC composites are similar, there are slight differences. Figure 4 shows the FT-IR spectra of the specimens, with bands at 3640 cm^{-1} and 3400 cm^{-1} present in all samples. These bands represent the stretching vibration of –OH in the organic components of SDBC (Park et al., 2018) and Si-OH in REC (Yao et al., 2014). In the composites, the peak at 3427 cm^{-1} is less pronounced compared to the sharp peak at 3390 cm^{-1} in REC. For SDBC, the peaks at 1614 cm^{-1}, 1438 cm^{-1}, 1029 cm^{-1}, and 787 cm^{-1} can be attributed to C=C and C=O, CH2, C-OH, and –CH groups, respectively (Deng et al., 2017; Wang and Wang, 2018; Zhang et al., 2013). The observed peaks at 530 cm^{-1} and 468 cm^{-1} may be due to the presence of aluminum salts in SDBC (Deng et al., 2017). In REC, the peaks at 1024 cm^{-1} and 546 cm^{-1}, 476 cm^{-1} are the result of stretching and bending vibrations of Si-OH, respectively. The peak at 918 cm^{-1} is likely due to the stretching vibration of Al-O-(OH)-Al (Wang et al., 2009). It should be noted that the peaks at

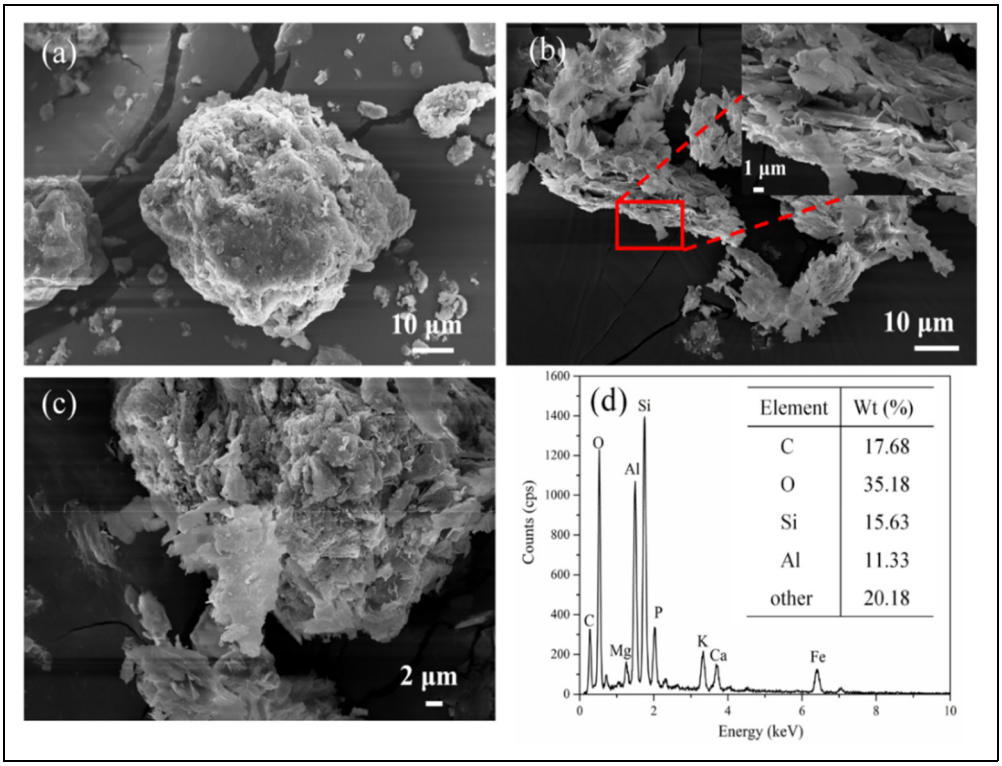

Figure 1. SEM images of SDBC (a), REC (b), and REC/SDBC composites (c) and EDS spectra of REC/SDBC composites (d).

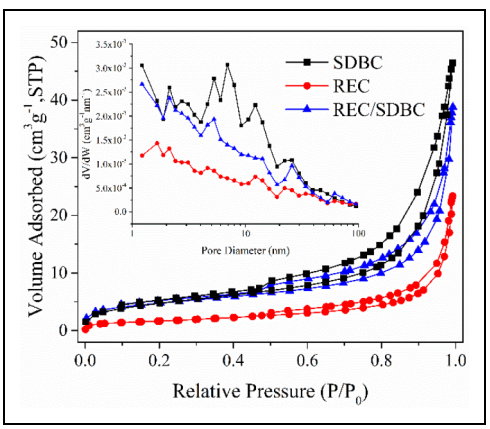

Figure 2. BET N_2 adsorption–desorption isotherms and the corresponding BJH pore size distribution plots (inset) of the obtained samples.

1629 cm^{-1} and 696 cm^{-1} in the FT-IR spectra are a combination of REC and SDBC. These results indicate that the REC/SDBC composites have been successfully fabricated and contain a variety of functional groups, which contribute to their effectiveness in removing Pb(II).

Adsorption kinetics

Before further examination of the adsorption performance of the as-prepared samples, SDBC, REC, and REC/SDBC composites with various mass ratios were selected to investigate the ability of Pb(II) removal. Figure 5 demonstrates the quantity of Pb(II) adsorbed by a series of specimens over time. The equilibrium adsorption capacities of Pb(II) are 24.06, 26.89, 25.95, and 24.53 mg g^{-1} for the REC/SDBC with mass ratios of 5:1, 3:1, 1:1, and 1:3, respectively. The Pb(II) adsorption capacities using REC/

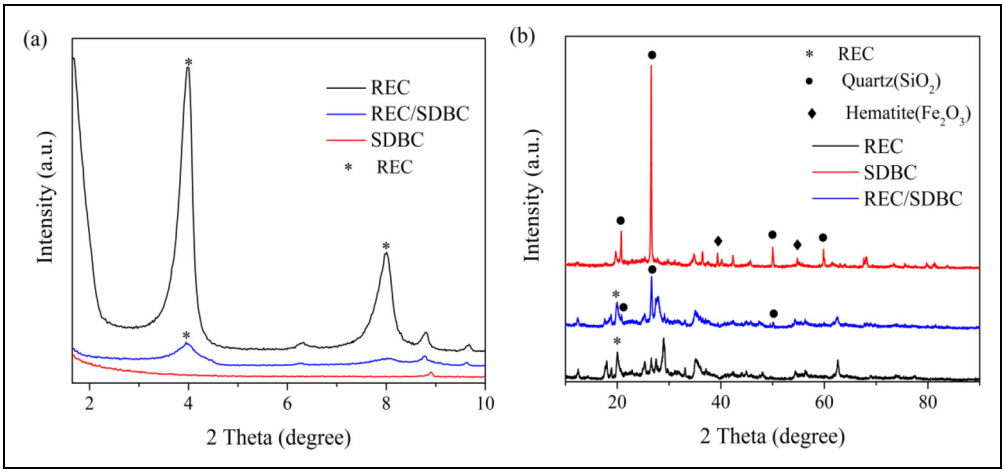

Figure 3. X-ray diffraction(XRD) patterns of the REC, SDBC, and REC/SDBC composites. (a) 2θ ranging from 2–10°, (b) 2θ ranging from 10–90°.

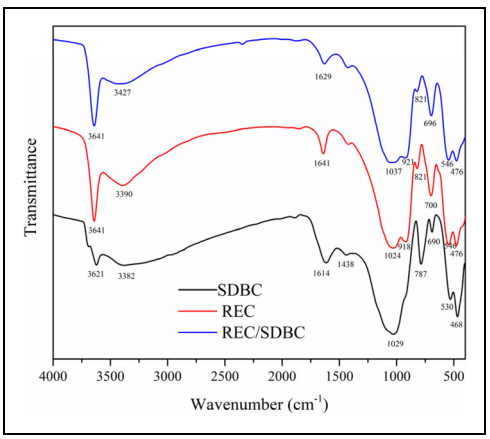

Figure 4. FT-IR spectra of the REC, SDBC, and REC/SDBC composites.

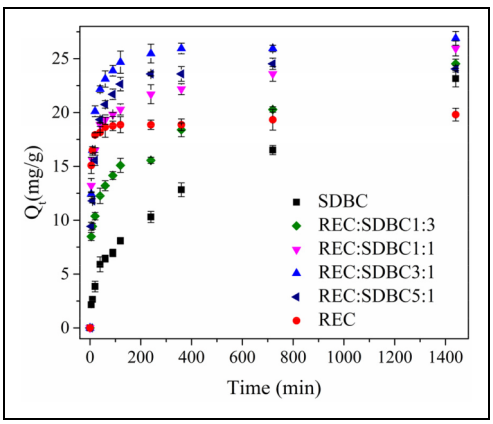

Figure 5. Adsorption kinetics of Pb(II) by REC, SDBC, and REC/SDBC composites with mass ratios of 5:1, 3:1, 1:1 and 1:3.

SDBC composites are invariably higher than that using SDBC (23.15 mg g^{-1}) and REC alone (19.81 mg g^{-1}). Besides, compared with the adsorption capacity of SDBC which increased continuously, REC/SDBC composites reached equilibrium mostly in 120 min. Especially when the mass ratio of REC/SDBC composites was 3:1, the adsorption capacity became as high as 26.89 mg g^{-1}, which is close to the median adsorption capacities (36.23 mg g^{-1}) of various clay minerals for Pb(II), ranging from 0.45 to 238.98 mg g^{-1} (Table S1, Supplementary Materials). Notably, the sorption capacity of the composite material is a little higher than the sum adsorption capacity of the individual components. For instance, the adsorption capacity for REC/SDBC composites with a mass ratio of 3:1 is 30% larger than the sum adsorption capacity of REC and SDBC with comparable mass in the composite ($23.15 \times 0.25 + 19.81 \times 0.75$). The preferential adsorption performance of Pb(II) by REC/SDBC composites originates from the synergism of REC and SDBC.

Table 3. Kinetic constants of REC, SDBC, and REC/SDBC composites for Pb(II) adsorption.

	Pseudo-first order			Pseudo-second order		
Adsorbents	$q_{1,cal}$ (mg g^{-1})	k_1 (min^{-1})	R^2	$q_{2,cal}$ (mg g^{-1})	k_2 (g min^{-1} mg^{-1})	R^2
SDBC	20.5428	0.0036	0.8824	24.0469	0.000176	0.9253
REC	18.7258	0.2971	0.9848	19.1513	0.0363	0.9972
REC/SDBC	24.6908	0.1111	0.9696	26.0453	0.0065	0.9963

Therefore, REC/SDBC composites with a mass ratio of 3:1 were selected for further investigation.

Pseudo-first-order (equation (2)) and pseudo-second-order (equation (3)) kinetic models were employed for describing the adsorption data in an attempt to analyze the adsorption process and mechanism of Pb(II) onto REC/SDBC composites (Wang et al., 2018; Wang and Wang, 2018; Xiao et al., 2018a):

$$q_t = q_e \times (1 - e^{-k_1 t}) \tag{2}$$

$$q_t = \frac{k_2 q_e^2 t}{1 + k_2 q_e t} \tag{3}$$

where k_1 and k_2 represent the constants for the first and second pseudo-order rates, respectively. Additionally, q_t and C denote the mass of Pb(II) adsorbed onto the adsorbent at time t and a constant reflecting the film thickness of intraparticle diffusion adsorption. The kinetic fitting models and fitting parameters are presented in Figure 6 and Table 3. Considering the higher coefficient of determination, the pseudo-second order kinetic model can better describe the process of Pb(II) adsorption onto REC and REC/SDBC composites. However, the adsorption rate of REC/SDBC (6.53×10^{-3} g min^{-1} mg^{-1}) composites is an order of magnitude lower than that of REC (3.63×10^{-2} g min^{-1} mg^{-1}), suggesting that the adsorption mechanisms are slightly different between REC and REC/SDBC composites.

Effects of pH

The removal efficiency of Pb(II) by REC/SDBC composites is influenced by the surface charge and initial solution pH. This is because cation exchange, surface complexation, and surface precipitation are the primary mechanisms responsible for the adsorption of Pb(II) onto REC/SDBC composites. Figure 9(a) shows the impact of starting solution pH (between 2 and 6) on the removal of Pb(II) by REC/SDBC composites. It is evident that the adsorption behavior is pH-dependent. The uptake of Pb(II) increases continuously as the pH increases, with a relatively low adsorption capacity (less than 10 mg g^{-1}) at pH 2–3. However, there is a sharp increase in adsorption capacity at pH 4, followed by a slower increase at pH above 5. This pH-dependent process can be attributed to the easier adsorption of more hydrolyzed Pb(II) compared to free Pb(II) (Li et al., 2017a; Ren et al., 2018) and the change in surface charge of the absorbent. Figure 9(b) shows that the surface of REC/SDBC composites is positively charged at pH < 3 but becomes more negatively charged as the pH increases. At pH 5, the decrease in zeta potential becomes much slower. This is mainly due to the deprotonation of surface functionalities reaching a maximum (Liang et al., 2017), which is consistent with the change in adsorption capacity. Therefore, as the pH increases, the electrical repulsion decreases, leading to an increase in adsorption capacity.

Adsorption isotherms

Figure 8 displays the findings of the investigation into the impact of the starting Pb(II)

concentration on the adsorption performance of Pb(II) onto REC/SDBC composites. The composites' adsorption capacity rises quickly at low concentrations before slowing down and progressively reaching equilibrium. Figure 8 depicts the simulation of the adsorption process using the Langmuir (equation (5)) and the Freundlich isotherm model (equation (6), with Table 4 listing the fitting parameters:

$$q_e = \frac{K_L q_m C_e}{1 + K_L C_e} \tag{5}$$

$$q_e = K_F C_e^{\frac{1}{n}} \tag{6}$$

where q_m represents the maximum adsorption capacity for monolayer coverage, KF, n, and KL are constants that depend on Freundlich, surface heterogeneity, and Langmuir, respectively. The Langmuir isotherm model better simulates the isotherm data, as indicated by its higher R^2 value. This suggests that the adsorption of Pb(II) onto the composites should result in monolayer coverage (Wang et al., 2018; Xiao et al., 2018a; Zhou et al., 2017b; Zhou et al., 2017c).

The dimensionless separation parameter RL is defined based on the Langmuir isotherm model, and can be calculated as follows:

$$R_L = \frac{1}{1 + K_L C_0} \tag{11}$$

whether or not the adsorption process is thermodynamically favorable is determined by the R_L value (Zhou et al., 2017a). The adsorption is not favored when $R_L > 1$, linear when $R_L = 1$, favorable when $1 > R_L > 0$, and $R_L = 0$ indicates that the adsorption is irreversible. The obtained R_L values in the current work have been listed in Table 4, in which all R_L values are in the range of 0–1, implying that the adsorption of Pb(II) onto the composites is favorable.

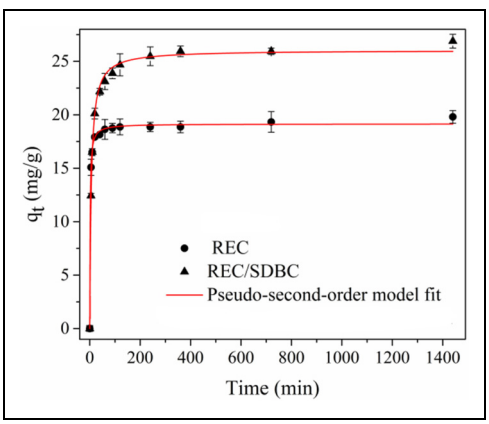

Figure 6. Kinetics of Pb(II) adsorption onto REC/SDBC composites.

Adsorption kinetics

The adsorption capacities of Pb(II) by REC/SDBC composites were investigated at varying temperatures of 293.15, 303.15, and 313.15 K in order to determine the effect of temperature on adsorption performance. As shown in Figure 6, the adsorption capacity of Pb(II) increases with higher temperatures, indicating an endothermic process (Wu et al., 2018). The thermodynamic parameters, including enthalpy (ΔH^0), Gibbs free energy (ΔG^0), and entropy (ΔS^0), can be calculated from the temperature-dependent adsorption isotherms

Table 4. Adsorption isotherm parameters of Pb(II) adsorption onto REC/SDBC composites.

	Langmuir isotherm model				Freundlich isotherm model		
Temperature (K)	q_m (mg g^{-1})	K_L (L mg^{-1})	R^2	R_L range	K_F (mg g^{-1} / (mg $L^{-1})^{1/n}$)	n	R^2
293.15	26.3787	0.3190	0.9825	0.0078–0.3854	11.5413	6.2147	0.9557
303.15	29.5153	0.2114	0.9723	0.0117–0.4861	11.1253	5.3390	0.9460
313.15	30.4748	0.2430	0.9763	0.0102–0.4509	12.1641	5.7770	0.9367

Table 5. Thermodynamic parameters of Pb(II) adsorption onto REC/SDBC composites.

Temperature (K)	ΔG^0 (KJ mol^{-1})	ΔH^0 (KJ mol^{-1})	ΔS^0 (J K^{-1} mol^{-1})
293.15	−1.4960	3.8177	18.0231
303.15	−1.5871		
313.1	−1.8564		

using the following equations (equations (12) and (13)):

$$\Delta G^0 = -RT \ln K^0 \tag{12}$$

$$\Delta G^0 = \Delta H^0 - T\Delta S^0 \tag{13}$$

where T represents temperature and R is the universal gas constant. By plotting ln Kd (where Kd = qe/Ce) against Ce and extrapolating Ce to zero, the thermodynamic equilibrium constant (K^0) can be calculated. The slope and intercept of the G^0-T curve can theoretically be used to determine ΔS^0 and $\Delta H0$, respectively (Li et al., 2017b; Radi et al., 2019; Renu et al., 2021). Table 5 presents a summary of the calculated parameter values. It is important to note that the adsorption process is thermodynamically favorable and spontaneous when the value of ΔG^0 is negative. Furthermore, the value of G^0 decreases with increasing temperature, indicating that a higher temperature is more conducive to the adsorption process. The endothermic nature of the adsorption process is also supported by the positive value of ΔH^0. Additionally, the positive value of S^0 suggests that the composites have a strong affinity for Pb(II) and that there is an increase in randomness at the solid/solution interface.

Adsorption mechanisms

The elemental chemical compositions and chemical states of the REC/SDBC composites were analyzed using XPS before and after adsorption to further support the potential mechanism of Pb(II) adsorption. Figure 7 displays the deconvolution of the high-resolution C 1 s, O 1 s, and Pb 4f peaks of the composites, as well as the XPS scan spectrum. The results of the elemental analysis are consistent with the major elements of the composites, namely C, O, Si, Al, and Na, as shown in Figure 7(a). The element Na, known for its strong cation exchange capabilities, could potentially substitute Pb(II), while surface functional groups containing C and O could also react with Pb(II) (Li et al., 2017b; Wang and Liu, 2018). Furthermore, the spectrum revealed two new Pb 4d and 4f peaks after Pb(II) adsorption, providing evidence for the effective adsorption of Pb(II) by the REC/SDBC composites (Figure 7(b)).

The high-resolution XPS spectrum of the composites' C 1 s peak was fitted into three peaks with binding energies at 284.7, 286.0, and 288.2 eV, corresponding to C-C, C-O, and O-C=O, respectively (Liu et al., 2011; Zhang et al., 2016; Zhou et al., 2017b). After Pb(II) adsorption, the binding energies of C-C and O-C=O shifted to higher values at 284.8 and 288.7 eV, and the peak area ratio of O-C=O decreased from 9.72% to 6.46%. These results confirm the involvement of carboxylic groups in the Pb(II) adsorption process and the formation of carboxyl-Pb complexes, consistent with previous studies (Zhang et al., 2016; Zhou et al., 2017b). In the high-resolution XPS spectrum of O 1 s, a pair of peaks at 531.7 and 532.4 eV, attributed to the oxygen groups of O-C=O and –OH, were observed (Wang and Liu, 2018). The –OH peak can originate from both organic functional groups (such as hydroxyl or ethers) and surface Si-OH groups. After adsorption, the binding energies of O-C=O and –OH shifted to 531.8 and 532.5 eV, and the peak area ratio of –OH decreased from 64.29% to 59.14% due to its involvement in Pb(II) adsorption. Additionally, a new peak at 530.8 eV was observed after

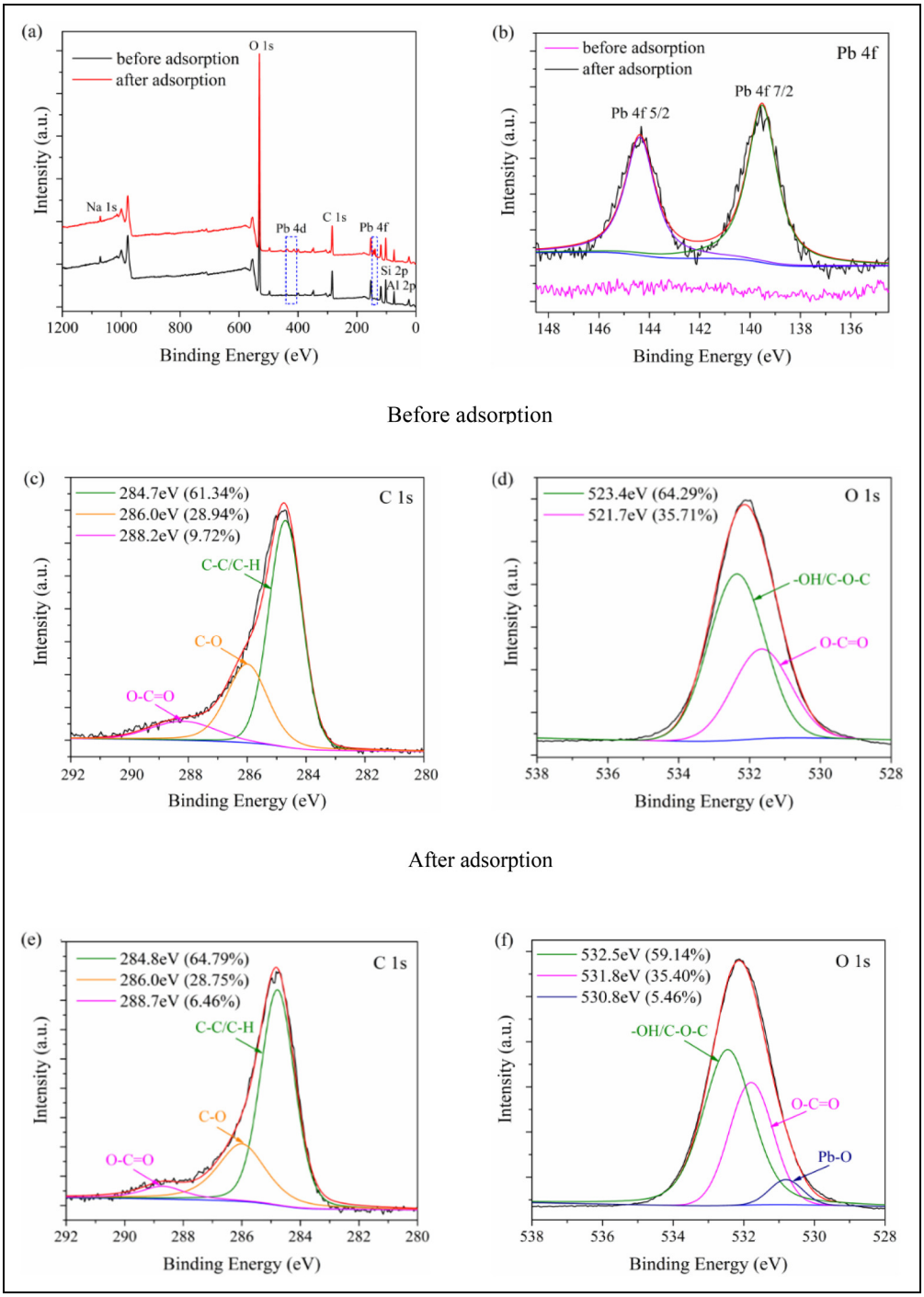

Figure 7. XPS survey spectra (a), high-resolution spectra of Pb 4f (b), C 1 s (c, e), O 1 s (d, f) of REC/SDBC composites before and after adsorption.

adsorption, assigned to the O 1 s in the Pb-O bond (Wang et al., 2007). These results suggest the formation of Pb-O bonds between Pb(II) and the surface functionalities of the composites. The Pb 4f spectrum of the composites before and after the reaction is shown in Figure 9(b). Prior to adsorption, no peaks of the Pb element were evident in the XPS spectrum of the composites. However, after adsorption, a set of peaks with binding energies at 139.5 and 144.4 eV were observed, corresponding to Pb-O and Pb-O-C, consistent with the O 1 s XPS analysis.

Overall, the XPS analysis shows that Pb(II) adsorption onto the REC/SDBC composites is a combination process involving cation exchange, surface complexation (Figure 10). Previous studies have demonstrated that Pb(II) adsorption by REC primarily involves electrostatic cation exchange and the formation of inner-sphere complexes at the edges of REC particles, facilitated by ≡Si-O- and ≡Al-O- groups (Celis et al., 2000).

Chemisorption, which includes surface complexation with free hydroxyl and carboxyl

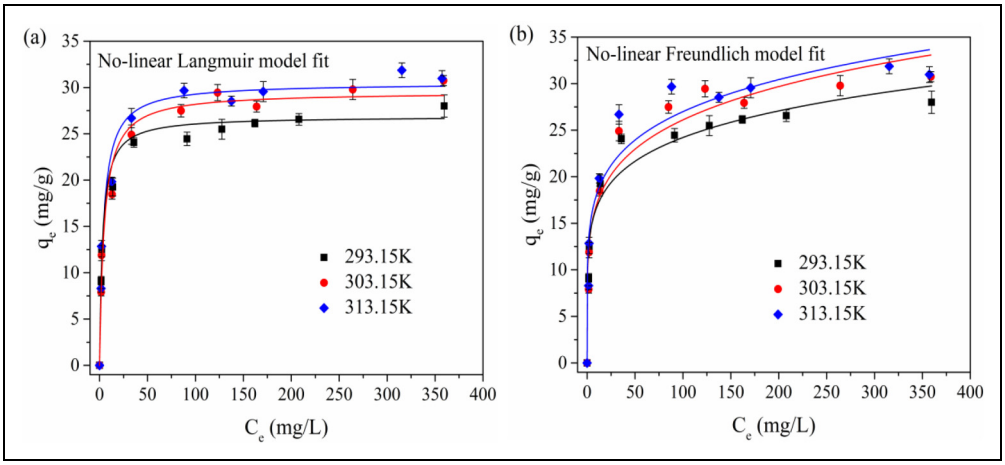

Figure 8. Adsorption isotherms for adsorption of Pb(II) by REC/SDBC composites.

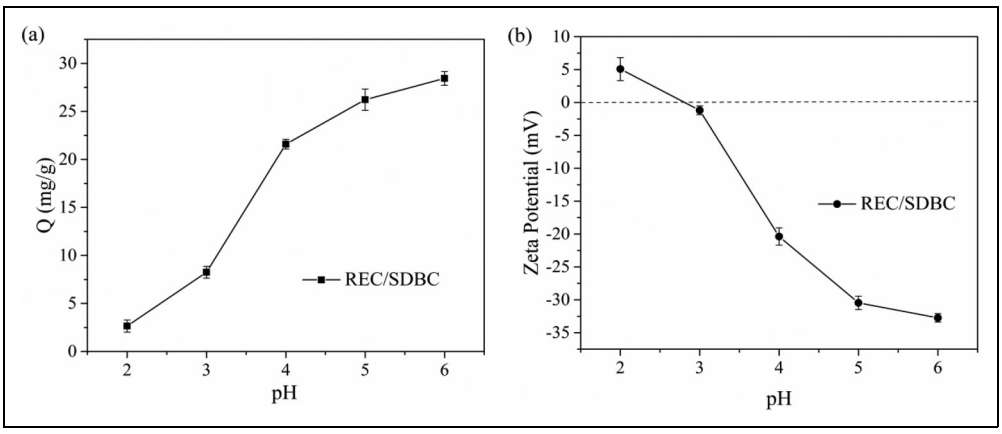

Figure 9. (a) Effects of initial pH on Pb(II) adsorption capacity; (b) Zeta pontentials of REC/SDBC composites at different pH values.

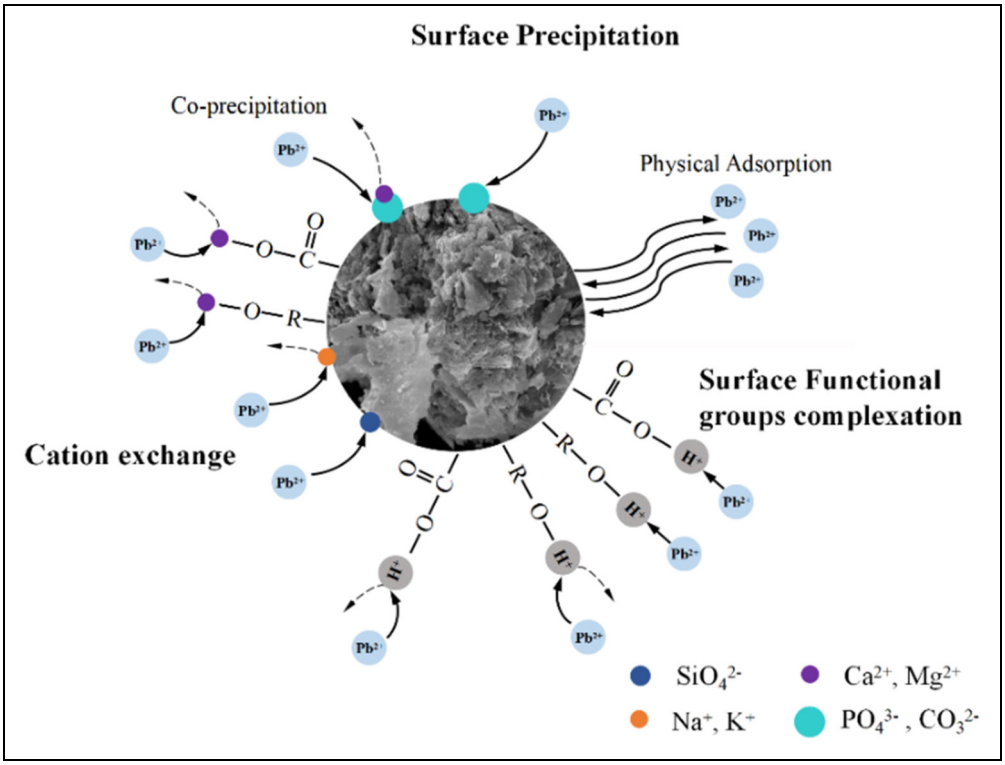

Figure 10. Schematic for the proposed mechanisms of Pb(II) adsorption onto REC/SDBC composites.

functional groups, surface precipitation, and cation exchange with interlayer Na^+ in the REC phase and Ca^{2+}, Mg^{2+} in the SDBC phase, also controls the adsorption of Pb(II) onto REC/SDBC composites. Nevertheless, the individual contribution to the adsorption was not quantified in the current study.

Conclusions

Novel and cost-effective REC/SDBC composites were successfully synthesized and thoroughly characterized. These composites exhibit a mesoporous structure, with a BET surface area of 16.5 m^2/g. The REC component possesses a layered structure, while most SDBC particles are amorphous and granular. In the REC/SDBC composites, REC is primarily dispersed on the surface of the SDBC particles. The composites demonstrated a significantly higher adsorption capacity compared to REC alone and reached equilibrium more rapidly than SDBC. The adsorption process was highly sensitive to pH, with equilibrium achieved within 120 min. Kinetic data were best described by the pseudo-second-order model. The adsorption mechanism for Pb(II) onto the REC/SDBC composites involves cation exchange, surface complexation, and surface precipitation. Additionally, the minimal changes observed in the structure of the REC/SDBC composites indicate their stability. These findings suggest that REC/SDBC composites are promising candidates for effectively treating Pb(II)-contaminated wastewater.

Author contributions

Conceptualization, H.W. and J.Z.; methodology, H.W.; software, J.Z., Z.W.; validation, J.W. and Z.W.; formal

analysis, J.Z.; data curation, J.Z.; writing—original draft preparation, H.W.; writing—review and editing, J.W. and Q.Y.; project administration, H.W. All authors have read and agreed to the published version of the manuscript.

Data availability statement

The authors confirm that the data supporting the findings of this study are available within the article and its supplementary materials.

Declaration of conflicting interests

The author(s) declared no potential conflicts of interest with respect to the research, authorship, and/or publication of this article.

Funding

The author(s) disclosed receipt of the following financial support for the research, authorship, and/or publication of this article: This research was funded by the Scientific Research Foundation for High-level Talents of West Anhui University (WGKQ2021014) and College Students' Innovative Entrepreneurial Training Plan Program "Preparation and performance study of rectorite-based phosphorus locking agents" (Grant No. S202110376103 and No. 202310376032).

ORCID iDs

Qing Ye https://orcid.org/0009-0004-9771-9608
Junye Zhang https://orcid.org/0000-0003-0030-9078

Supplemental material

Supplemental material for this article is available online.

References

Abdul G, Zhu XY and Chen BL (2017) Structural characteristics of biochar-graphene nanosheet composites and their adsorption performance for phthalic acid esters. *Chemical Engineering Journal* 319: 9–20.

Abdulkarim M and Abu Al-Rub F (2004) Adsorption of lead ions from aqueous solution onto activated carbon and chemically-modified activated carbon prepared from date pits. *Adsorption Science & Technology* 22(2): 119–134.

Bai XP, Wang GH, Gong CX, et al. (2017) Co-pelletizing characteristics of torrefied wheat straw with peanut shell. *Bioresource Technology* 233: 373–381.

Bordoloi N, Goswami R, Kumar M, et al. (2017) Biosorption of Co (II) from aqueous solution using algal biochar: Kinetics and isotherm studies. *Bioresource Technology* 244: 1465–1469.

Cao XD, Ma LN, Liang Y, et al. (2011) Simultaneous immobilization of lead and atrazine in contaminated soils using dairy-manure biochar. *Environmental Science & Technology* 45(11): 4884–4889.

Celis R, Hermosín MC and Cornejo J (2000) Heavy metal adsorption by functionalized clays. *Environmental Science & Technology* 34(21): 4593–4599.

Chen BL, Zhou DD and Zhu LZ (2008) Transitional adsorption and partition of nonpolar and polar aromatic contaminants by biochars of pine needles with different pyrolytic temperatures. *Environmental Science & Technology* 42(14): 5137–5143.

Chen L, Chen XL, Zhou CH, et al. (2017) Environmental-friendly montmorillonite-biochar composites: Facile production and tunable adsorption-release of ammonium and phosphate. *Journal of Cleaner Production* 156: 648–659.

Chen YF, Fang JZ, Lu SY, et al. (2015) Plasmonic Ag-pillared rectorite as catalyst for degradation of 2,4-DCP in the H2O2-containing system under visible light irradiation. *Journal of Hazardous Materials* 297: 278–285.

Chen ZM, Chen BL and Chiou CT (2012) Fast and slow rates of naphthalene sorption to biochars produced at different temperatures. *Environmental Science & Technology* 46(20): 11104–11111.

Damdib S, , Siyasukh A and , Vanichsetakul B, et al. (2023) Efficient removal of paraquat pollutants using magnetic biochar derived from corn husk waste: A sustainable approach for water remediation. *Adsorption Science & Technology*. DOI:10.1155/2023/55128812023.

Deng JQ, Liu YQ, Liu SB, et al. (2017) Competitive adsorption of Pb(II), Cd(II) and Cu(II) onto chitosan-pyromellitic dianhydride modified biochar. *Journal of Colloid and Interface Science* 506: 355–364.

Dhyani V, Awasthi MK, Wang Q, et al. (2018) Effect of composting on the thermal decomposition behavior

and kinetic parameters of pig manure-derived solid waste. *Bioresource Technology* 252: 59–65.

Dias D, Lapa N, Bernardo M, et al. (2017) Properties of chars from the gasification and pyrolysis of rice waste streams towards their valorisation as adsorbent materials. *Waste Management* 65: 186–194.

Dias D, Lapa N, Bernardo M, et al. (2018) Cr(III) removal from synthetic and industrial wastewaters by using co-gasification chars of rice waste streams. *Bioresource Technology* 266: 139–150.

Edo C, González-Pleiter M, Leganés F, et al. (2020) Fate of microplastics in wastewater treatment plants and their environmental dispersion with effluent and sludge. *Environmental Pollution* 259: 113837.

Fang WC, Cheng XX, Sun CJ, et al. (2023) Optimization of the fabrication of sustainable ceramsite adsorbent from coal fly ash/waterworks sludge/waste glass for decolorization of malachite green. *Adsorption Science & Technology* 2023. DOI: 10.1155/2023/8581697.

Gao NB, Kamran K, Quan C, et al. (2020) Thermochemical conversion of sewage sludge: A critical review. *Progress in Energy and Combustion Science* 79: 100843.

He JS, Cui AA, Deng SH, et al. (2018) Treatment of methylene blue containing wastewater by a cost-effective micro-scale biochar/polysulfone mixed matrix hollow fiber membrane: Performance and mechanism studies. *Journal of Colloid and Interface Science* 512: 190–197.

Hoang SA, Bolan N, Madhubashani AMP, et al. (2022) Treatment processes to eliminate potential environmental hazards and restore agronomic value of sewage sludge: A review. *Environmental Pollution* 293. DOI: 10.1016/j.envpol.2021.118564.

Huang H, Yao WL, Li RH, et al. (2018) Effect of pyrolysis temperature on chemical form, behavior and environmental risk of Zn, Pb and Cd in biochar produced from phytoremediation residue. *Bioresource Technology* 249: 487–493.

Inyang M, Gao B, Zimmerman A, et al. (2014) Synthesis, characterization, and dye sorption ability of carbon nanotube-biochar nanocomposites. *Chemical Engineering Journal* 236: 39–46.

Kah M, Sigmund G, Xiao F, et al. (2017) Sorption of ionizable and ionic organic compounds to biochar, activated carbon and other carbonaceous materials. *Water Research* 124: 673–692.

Li HB, Dong XL, da Silva EB, et al. (2017a) Mechanisms of metal sorption by biochars: Biochar characteristics and modifications. *Chemosphere* 178: 466–478.

Li J, Yu GW, Xie SY, et al. (2018a) Immobilization of heavy metals in ceramsite produced from sewage sludge biochar. *Science of the Total Environment* 628–629: 131–140.

Li M, Tang YY, Ren NN, et al. (2018b) Effect of mineral constituents on temperature-dependent structural characterization of carbon fractions in sewage sludge-derived biochar. *Journal of Cleaner Production* 172: 3342–3350.

Li MF, Liu YG, Liu SB, et al. (2017b) Cu(II)-influenced adsorption of ciprofloxacin from aqueous solutions by magnetic graphene oxide/nitrilotriacetic acid nanocomposite: Competition and enhancement mechanisms. *Chemical Engineering Journal* 319: 219–228.

Li Y, Wang ZW, Xie XY, et al. (2017c) Removal of Norfloxacin from aqueous solution by clay-biochar composite prepared from potato stem and natural attapulgite. *Colloids and Surfaces A-Physicochemical and Engineering Aspects* 514: 126–136.

Liang J, Li XM, Yu ZG, et al. (2017) Amorphous MnO_2 modified biochar derived from aerobically composted swine manure for adsorption of Pb(II) and Cd(II). *Acs Sustainable Chemistry & Engineering* 5(6): 5049–5058.

Liu WJ, Jiang H and HQ Y (2015) Development of biochar-based functional materials: Toward a sustainable platform carbon material. *Chemical Reviews* 115(22): 12251–12285.

Liu WJ, Zeng FX, Jiang H, et al. (2011) Adsorption of lead (Pb) from aqueous solution with Typha angustifolia biomass modified by $SOCl_2$ activated EDTA. *Chemical Engineering Journal* 170(1): 21–28.

Liu XJ, Lai DG and Wang Y (2019) Performance of Pb(II) removal by an activated carbon supported nanoscale zero-valent iron composite at ultralow iron content. *Journal of Hazardous Materials* 361: 37–48.

Liu XY, Zhu FF, Zhang RY, et al. (2021) Recent progress on biodiesel production from municipal sewage sludge. *Renewable & Sustainable Energy Reviews* 135: 110260.

Lyu HH, Gao B, He F, et al. (2018) Experimental and modeling investigations of ball-milled biochar for the removal of aqueous methylene blue. *Chemical Engineering Journal* 335: 110–119.

Pan XQ, Gu ZP, Chen WM, et al. (2021) Preparation of biochar and biochar composites and their application in a Fenton-like process for wastewater decontamination: A review. *Science of the Total Environment* 754: 142104.

Park JL, Wang JJ, Xiao R, et al. (2018) Effect of pyrolysis temperature on phosphate adsorption characteristics and mechanisms of crawfish char. *Journal of Colloid and Interface Science* 525: 143–151.

Radi S, El Abiad C, Moura NMM, et al. (2019) New hybrid adsorbent based on porphyrin functionalized silica for heavy metals removal: Synthesis, characterization, isotherms, kinetics and thermodynamics studies. *Journal of Hazardous Materials* 370: 80–90.

Ren NN, Tang YY and Li M (2018) Mineral additive enhanced carbon retention and stabilization in sewage sludge-derived biochar. *Process Safety and Environmental Protection* 115: 70–78.

Renu K, Chakraborty R, Myakala H, et al. (2021) Molecular mechanism of heavy metals (Lead, Chromium, Arsenic, Mercury, Nickel and Cadmium)—induced hepatotoxicity—A review. *Chemosphere* 271: 129735.

Song M, Wei YX, Cai SP, et al. (2018) Study on adsorption properties and mechanism of Pb^{2+} with different carbon based adsorbents. *Science of the Total Environment* 618: 1416–1422.

Tang L, Yu JF, Pang Y, et al. (2018) Sustainable efficient adsorbent: Alkali-acid modified magnetic biochar derived from sewage sludge for aqueous organic contaminant removal. *Chemical Engineering Journal* 336: 160–169.

Tang S, Lin LJ, Wang XS, et al. (2020) Pb(II) uptake onto nylon microplastics: Interaction mechanism and adsorption performance. *Journal of Hazardous Materials* 386: 121960.

Uddin MK (2017) A review on the adsorption of heavy metals by clay minerals, with special focus on the past decade. *Chemical Engineering Journal* 308: 438–462.

Wang CQ and Wang H (2018) Pb(II) sorption from aqueous solution by novel biochar loaded with nano-particles. *Chemosphere* 192: 1–4.

Wang DF, Guo W, Zhang GL, et al. (2017a) Remediation of Cr(VI)-contaminated acid soil using a nanocomposite. *Acs Sustainable Chemistry & Engineering* 5(3): 2246–2254.

Wang HJ, Zhou AL, Peng F, et al. (2007) Mechanism study on adsorption of acidified multiwalled carbon nanotubes to Pb(II). *Journal of Colloid and Interface Science* 316(2): 277–283.

Wang SW, Dong YH, He ML, et al. (2009) Characterization of GMZ bentonite and its application in the adsorption of Pb(II) from aqueous solutions. *Applied Clay Science* 43(2): 164–171.

Wang X, Huang K, Chen Y, et al. (2018) Preparation of dumbbell manganese dioxide/gelatin composites and their application in the removal of lead and cadmium ions. *Journal of Hazardous Materials* 350: 46–54.

Wang Y and Liu RH (2018) H_2o_2treatment enhanced the heavy metals removal by manure biochar in aqueous solutions. *Science of the Total Environment* 628–629: 1139–1148.

Wang YG, Hu LH, Zhang GY, et al. (2017b) Removal of Pb(II) and methylene blue from aqueous solution by magnetic hydroxyapatite-immobilized oxidized multi-walled carbon nanotubes. *Journal of Colloid and Interface Science* 494: 380–388.

Woolf D, Amonette JE, Street-Perrott FA, et al. (2010) Sustainable biochar to mitigate global climate change. *Nature Communications* 1. DOI: 10.1038/ncomms1053.

Wu D, Hu LH, Wang YG, et al. (2018) EDTA Modified β-cyclodextrin/chitosan for rapid removal of Pb(II) and acid red from aqueous solution. *Journal of Colloid and Interface Science* 523: 56–64.

Wu DL, Zheng PW, Chang PR, et al. (2011) Preparation and characterization of magnetic rectorite/iron oxide nanocomposites and its application for the removal of the dyes. *Chemical Engineering Journal* 174(1): 489–494.

Wu SH, He HJ, Inthapanya X, et al. (2017) Role of biochar on composting of organic wastes and remediation of contaminated soils-a review. *Environmental Science and Pollution Research* 24(20): 16560–16577.

Xiao BY, Dai Q, Yu X, et al. (2018a) Effects of sludge thermal-alkaline pretreatment on cationic red X-GRL adsorption onto pyrolysis biochar of sewage sludge. *Journal of Hazardous Materials* 343: 347–355.

Xiao R, Wang JJ, Li RH, et al. (2018b) Enhanced sorption of hexavalent chromium Cr(VI) from aqueous solutions by diluted sulfuric acid-assisted MgO-coated biochar composite. *Chemosphere* 208: 408–416.

Xu DF, Cheng B, Wang WK, et al. (2018) Ag_2/CrO_4/g-C_3N_4/graphene oxide ternary nanocomposite Z-scheme photocatalyst with enhanced CO_2 reduction activity. *Applied Catalysis B-Environmental* 231: 368–380.

Yang F, Sun LL, Xie WL, et al. (2017) Nitrogen-functionalization biochars derived from wheat straws via molten salt synthesis: An efficient adsorbent for atrazine removal. *Science of the Total Environment* 607–608: 1391–1399.

Yao Y, Gao B, Fang JN, et al. (2014) Characterization and environmental applications of clay-biochar composites. *Chemical Engineering Journal* 242: 136–143.

Zhang C, Lai C, Zeng GM, et al. (2016) Efficacy of carbonaceous nanocomposites for sorbing ionizable antibiotic sulfamethazine from aqueous solution. *Water Research* 95: 103–112.

Zhang GK, Gao YY, Zhang YL, et al. (2010) Fe_2O_3-pillared rectorite as an efficient and stable Fenton-like heterogeneous catalyst for photodegradation of organic contaminants. *Environmental Science & Technology* 44(16): 6384–6389.

Zhang JC, He YW, Fang YC, et al. (2021) Characteristics and influencing factors of microbial community in heavy metal contaminated soil under silicon fertilizer and biochar remediation. *Adsorption Science & Technology* 2021. DOI: 10.1155/2021/9964562.

Zhang WH, Mao SY, Chen H, et al. (2013) Pb(II) and Cr(VI) sorption by biochars pyrolyzed from the municipal wastewater sludge under different heating conditions. *Bioresource Technology* 147: 545–552.

Zhou N, Chen HG, Feng QJ, et al. (2017a) Effect of phosphoric acid on the surface properties and Pb(II) adsorption mechanisms of hydrochars prepared from fresh banana peels. *Journal of Cleaner Production* 165: 221–230.

Zhou N, Chen HG, Xi JT, et al. (2017b) Biochars with excellent Pb(II) adsorption property produced from fresh and dehydrated banana peels via hydrothermal carbonization. *Bioresource Technology* 232: 204–210.

Zhou YY, Liu XC, Tang L, et al. (2017c) Insight into highly efficient co-removal of p-nitrophenol and lead by nitrogen-functionalized magnetic ordered mesoporous carbon: Performance and modelling. *Journal of Hazardous Materials* 333: 80–87.